A Model Investigation of Aerosol-induced Changes in Tropical Circulation

Yi Ming * and V. Ramaswamy

Geophysical Fluid Dynamics Laboratory/NOAA, Princeton, NJ

* *Corresponding author address:* Yi Ming, Geophysical Fluid Dynamics Laboratory/NOAA, P. O. Box 308, Princeton, NJ 08542.

E-mail: Yi.Ming@noaa.gov

ABSTRACT

We study how anthropogenic aerosols, alone or in conjunction with radiatively active gases, affect the tropical circulation with an atmosphere/mixed layer ocean general circulation model. Aerosol-induced cooling gives rise to a substantial increase in the overall strength of the tropical circulation, a robust outcome consistent with a thermodynamical scaling argument. Owing to the interhemispheric asymmetry in aerosol forcing, the zonal-mean and zonally asymmetrical components of the tropical circulation respond differently. The Hadley circulation weakens in the Northern Hemisphere, but strengthens in the Southern Hemisphere. The resulting northward cross-equatorial moist static energy flux compensates partly for the aerosol radiative cooling in the Northern Hemisphere. In contrast, the less restricted zonally asymmetrical circulation does not show sensitivity to the spatial structure of aerosols, and strengthens in both hemispheres. Our results also point to the possible role of aerosols in driving the observed reduction in the equatorial sea level pressure gradient.

These circulation changes have profound implications for the hydrological cycle. We find that aerosols alone make the subtropical dry zones in both hemispheres wetter, as the local hydrological response is controlled thermodynamically by atmospheric moisture content. The deep tropical rainfall undergoes a dynamically induced southward shift, a robust pattern consistent with the adjustments in the zonal-mean circulation and in the meridional moist static energy transport. Less certain is the magnitude of the shift. The nonlinearity exhibited by the combined hydrological response to aerosols and radiatively active gases is dynamical in nature.

1. Introduction

Although much remains to be done to gain a more definitive understanding of the climate effects of aerosols (radiative and microphysical alike) (e.g., Forster et al. 2007), it has been widely accepted that aerosol cooling "masked", on the global scale, a considerable fraction of greenhouse gas warming since the preindustrial times (e.g., Hegerl et al. 2007). Unlike well-mixed greenhouse gases, the spatial distributions of aerosols are highly non-uniform owing to inhomogeneous emission sources and short lifetimes (on the order of days). This basic recognition leads one to speculate that aerosols may be more capable of altering atmospheric and oceanic circulation, especially on the regional scale, than greenhouse gases. Despite a few early attempts (e.g., Ramaswamy and Chen 1997; Rotstayn and Lohmann 2002), aerosol impacts on the general circulation and hydrological cycle have not been studied in a systematic manner. This poses an acute need for research as the community strives to understand regional climate change for policy purposes.

When discussing how an external forcing, which is small relative to insolation, alters regional climate, one can argue that the response is more likely to be a deviation from the initial state within the same climate regime, as opposed to a complete shift from one climate regime to another. It is also conceivable that the response to the same forcing may vary with underlying climate regime. For example, as a result of the smallness of the Coriolis parameter, the tropics can efficiently remove strong horizontal temperature gradients through internal gravity waves (Sobel et al. 2001). Thus, the thermal influence of a regional forcing may be spread throughout the tropics. The opposite is true in the extratropics, where the influence is more likely to be kept local by adjusting zonal winds. This reasoning motivates us to investigate, in a series of three papers, how aerosols affect the circulation patterns in different climate zones. This paper focuses on the tropical circulation, while the other two are devoted to the monsoon and boreal winter extratropical circulations, respectively (Ming et al. 2011a,b).

Theories and general circulation model (GCM) simulations were key to developing fundamental insights into how the circulation and precipitation would vary in response to global warming (e.g., Held and Soden 2006, referred to as HS06). At the heart of HS06 is a thermodynamical scaling argument based on the mass balance of water in the free troposphere, which dictates

$$\delta M_c/M_c = \delta P/P - \alpha \delta T, \tag{1}$$

where M_c is the convective mass flux out of the boundary layer, P is precipitation, and T is surface temperature, all in global-mean. α is constant at 0.07 K^{-1} according to the Clausius-Clapeyron scaling of the saturated water vapor pressure. Because P is constrained by the approximate balance between atmospheric radiative cooling and convective heating to increase by 1 - 3% for one degree of surface warming (Allen and Ingram 2002; Stephens and Ellis 2008), M_c has to decrease by 4 - 6%. This reduction in convective mass is manifested as a weakening of the tropical circulation in GCM (HS06; Vecchi and Soden 2007). It is worth noting that an observationally-based study by Liu et al. (2009) suggested that the global average precipitation increased with temperature at a rate far greater than projected by GCM. If confirmed, this finding would point toward serious deficiencies in model formulations.

One immediate question is to what extent this thermodynamical scaling argument is applicable to aerosol-induced changes in the tropical-mean circulation and in its zonal-mean (Hadley) and zonally asymmetrical components. We seek the answers using a set of atmosphere/mixed-layer ocean GCM simulations of the equilibrium climate response to aerosols. We also examine the role of aerosols, if any, in affecting the spatial pattern of the tropical sea level pressure (SLP). HS06 showed that the regional precipitation change caused by global warming is governed mainly by the Clausius-Clapeyron scaling of atmospheric moisture content. We investigate whether this is still the case in the event of substantial modification of flow by non-uniform aerosols, and further discuss the underlying mechanism of the nonlinearity in the combined hydrological response to aerosols and greenhouse gases (Ming and Ramaswamy 2009, referred to as MR09).

2. Tropical-mean Circulation

The atmospheric component of the coupled GCM is a modified version of the Geophysical Fluid Dynamics Laboratory (GFDL) AM2.1 atmosphere GCM (The GFDL Global Atmospheric Model Development Team 2004), which implements a prognostic scheme of cloud droplet number concentration for taking into account aerosol indirect effects (Ming et al. 2007). The initial droplet number concentration in a newly formed cloud is linked to aerosol chemical composition, size distribution and mass concentration using a first principles-based parameterization of droplet activation (Ming et al. 2006). This applies both to large-scale clouds and to convective clouds. Three aerosol types, namely sulfate, organic carbon (OC) and sea salt, act as cloud condensation nuclei (CCN). All the prognostic cloud variables, including droplet number concentration, are transported and removed by the same dynamical, physical and microphysical processes.

The model uses as inputs the offline atmospheric aerosol burdens of sulfate, black carbon (BC), OC, dust and sea salt, all of which except that of sea salt are simulated using a chemical transport model driven by GCM-generated meteorological fields (Horowitz 2006). The fossil fuel emissions are based on EDGAR v2.0 (Olivier et al. 1996), with the exceptions of those of BC and OC, which follow Cooke et al. (1999). The tropical and extratropical biomass burning emissions are from Hao and Liu (1994) and Müller (1992), respectively, with the emission factors as specified in Andreae and Merlet (2001). The concentration of sea salt is computed from satellite-retrieved surface wind speed, and is assumed to be constant throughout the marine boundary layer (Haywood et al. 1999). As a result of relatively short lifetimes, the atmospheric concentrations of anthropogenic aerosols are highest over the Northern Hemisphere (NH) mid-latitude industrial regions (i.e., East Asia, North America and Europe) and over the tropical biomass burning regions (most notably Central Africa and South America), and decrease gradually as one moves away from the sources (see Figs. 4 and 5 of Horowitz (2006)). The simulated aerosol concentrations and optical depth were found to be in reasonably good agreement with field and satellite measurements (Ginoux et al. 2006).

The preindustrial control case (CONT) is run to equilibrium before being perturbed by present-day aerosols (AERO), by present-day radiatively active gases (greenhouse gases and ozone) (GAS), and by present-day aerosols and gases simultaneously (BOTH). Each case is integrated for 100 model years; the last 80 years are used for computing annual-mean changes and associated statistical significance based on the Student's *t*-test. The aerosol direct and indirect effects, evaluated as radiative flux perturbation (i.e., the change in the TOA radiative flux after atmospheric adjustment) (Hansen et al. 2005; Haywood et al. 2009), amount to a global-mean of -2.1 W m^{-2}. This includes a direct effect of -0.6 W m^{-2} and an indirect effect of -1.7 W m^{-2}. It is clear that the overall aerosol cooling results mainly from the indirect effects. Like the atmospheric burdens of anthropogenic aerosols, their radiative effects are located predominantly over the NH source regions. The reader is referred to MR09 for a more detailed description of the model configuration and design of the experiments.

Table 1 lists the tropical-mean changes in T, P and M_c due to different perturbations. Note that the tropics is defined as 30°S - 30°N in this study. It is reassuring to see that the model-simulated P increases with T at a rate of 2.2% K^{-1} in GAS (termed as *unadjusted* hydrological sensitivity in this study). This is consistent with other models, and is presumed to be dictated by the need to balance radiative cooling with convective heating (Allen and Ingram 2002). M_c lowers by 4.9% K^{-1}, satisfying the thermodynamical scaling (Eq. 1). As explained in HS06, if the tropical-mean circulation is conceptualized as convective ascent being balanced by radiatively driven subsidence, a redistribution of M_c alone (without changing its mean) can alter the circulation. In this sense, the spatial variance of M_c ($var(M_c)$) is a more reliable measure of the strength of the convective branch of the overall circulation. In response to radiatively active gases, $var(M_c)$ decreases by 8.8% K^{-1}, which is close to being twice of the rate of M_c (Table 1). This suggests that the fractional change in M_c is rather uniform across the tropics.

Aerosols lead to a surface cooling of 1.5 K along with a reduction in P of 5.7%. The normalized rate of 3.8% K^{-1} is considerably higher than that for greenhouse gases (2.2% K^{-1}), seemingly suggesting that the hydrological sensitivity differs between two types of forcing. As explained in Ming et al. (2010) and Andrews et al. (2010), the total δP can be separated approximately into two components. The fast atmosphere-only component results from the change in atmospheric radiative absorption (in shortwave for absorbing aerosols and in longwave for greenhouse gases) caused directly by a forcing agent, and thus does not scale with δT. The other component, which is manifested much more slowly than the atmosphere-only component, arises from the necessity of balancing the change in radiative cooling as the temperature of the coupled atmosphere-surface system adjusts to the forcing, and thus scales with δT. A set of simulations based on the same atmosphere GCM, but being forced with prescribed sea surface temperature and sea ice, suggest that precipitation lowers, incidentally, by the same percentage (1.2%) for aerosols and for greenhouse gases (i.e., the fast atmosphere-only component). By subtracting the fast component from the total δP, one can derive the slowly varying component, which amounts to a decrease of 4.5% for aerosols and an increase of 6.0% for greenhouse gases. The respective adjusted hydrological sensitivity, which is defined on the basis of the slow δT-related δP, is 3.0 and 2.7% K^{-1}. Note that the *adjusted* hydrological sensitivity is reasonably consistent across forcings, which is fundamentally owing to the radiative control of precipitation (Allen and Ingram 2002).

For aerosols, P, even with the atmosphere-only component included, still decreases with T at a pace (3.8% K^{-1}) slower than the Clausius-Clapeyron scaling (7% K^{-1}). The simulated M_c increases by 4.5%, which translates into a normalized rate of 3.0% K^{-1}, effectively following the thermodynamical scaling (Eq. 1). The increase in $var(M_c)$ (11.7%) is considerably more than twice of the increase in M_c, an indication of spatially uneven circulation changes. The conclusion that the tropical-mean circulation strengthens in response to aerosols is in line with the expectation from the thermodynamical scaling argument. The applicability of the scaling to aerosol-induced circulation changes is not surprising given the fact that it is based on the mass balance of moisture, which always holds at climate-relevant time scales due to the limited storage in the free troposphere.

3. Zonal-mean and Zonally asymmetrical Circulations

How is the aerosol-induced change in the overall circulation strength realized by modifying regional air flow? An examination of the differences in meridional stream function yields that a closed clockwise circulation centers roughly at the equator and spans over the deep tropics (15°S - 15°N) (Fig. 1). The associated flow acts to weaken the rising branch of the NH zonal-mean circulation, while strengthening its SH counterpart. It is accompanied by cross-equatorial northerlies in the lower troposphere. The returning flow is manifested as southerlies in the upper troposphere. Fig. 2 shows that the largest reductions in large-scale ascent (ω) occur mainly over the regions with the strongest ascent in CONT, namely the Intertropical Convergence Zone (ITCZ), West Pacific Warm Pool (WPWP) and Atlantic Warm Pool (AWP). The ascent over the SH convergence zones is enhanced substantially, and the dipole pattern marks a pronounced shift of the South Pacific Convergence Zone (SPCZ). However, it is not self-evident whether such a shift is meridional (equatorward), zonal (eastward), or a combination of both. It is equally unclear whether there are changes in the mean locations and/or areas of the other convergence zones including ITCZ. A later analysis will help clarify these issues. The large-scale descent is weaker over the NH subtropical subsidence regions (mainly the eastern part of the North Pacific), and is stronger over the SH counterparts (mainly the eastern part of the South Pacific). Since the hemispheric mean circulation is approximately closed, these changes in large-scale motion are in the opposite sign to those over the convective regions in the same hemisphere.

We now turn to the change in M_c caused by aerosols. Fig. 3(a) shows that M_c generally reduces over the convective regions in NH, but increases over those in SH. A comparison with Fig. 2 indicates that the spatial patterns of δM_c and $\delta\omega$ are closely tied, with faster grid-mean ascent collocating with stronger M_c, and vice versa. Fig. 3(b) plots the zonal-mean δM_c at a specific latitude across the zonal band, and Fig. 3(c) plots the residual after subtracting the zonal-mean from the total δM_c, which can be thought of as the zonally asymmetrical part of δM_c. (We intentionally choose to present the zonal-mean δM_c in a latitude-longitude plot, as opposed to a line plot, to facilitate a comparison with the zonally asymmetrical δM_c location by location.) The zonal-mean M_c lowers consistently between 5 - 20°N with largest reductions at around 10°N (over ITCZ and parts of WPWM and AWM). It increases virtually over the entire SH tropics with a maximum at around 10°S (over SPCZ and other SH convergence zones). Note that none of the convective belts undergoes a zonally wide meridional shift.

The zonally asymmetrical component of M_c generally reduces over the relatively narrow regions with the strongest convection such as WPWP and SPCZ, but increases considerably at the edges (e.g., the south side of ITCZ and east side of SPCZ). We characterize this pattern as flattening of the zonally asymmetrical circulation, which involves a re-distribution of convective mass mostly within the convergence zones. The fundamental mechanism underlying the shift of convective activities is still unclear, and will be a subject of further study.

One can examine this issue further by decomposing the tropical-mean change in $var(M_c)$ into the zonal-mean (Hadley) and zonally asymmetric components in both hemispheres (Table 2). Following the thermodynamical scaling, all four components weaken in GAS, but the zonally asymmetrical circulation experiences a much greater reduction in strength than the zonal-mean circulation. This result is common among models, and can be thought of as a consequence of the zonal-mean circulation being more restricted (HS06).

The zonal-mean circulation responds to aerosols differently between the hemispheres; it weakens by 15.8% in NH, but strengthens by 30.4% in the Southern Hemisphere (SH). We presume that this pattern, which is distinct from GAS, results from uneven aerosol distribution between two hemispheres, and will revisit it in Section 5. In marked contrast, the zonally asymmetrical circulation strengthens in both hemispheres to an extent comparable to the tropical-mean. This seems to suggest that the way in which the zonally asymmetrical circulation adjusts to a perturbation (either greenhouse gases or aerosols) is linked tightly to the tropical-mean temperature change according to the thermodynamical scaling. The adjustment is insensitive to the spatial structures of the perturbation and subsequent temperature change.

4. Sea Level Pressure

From the thermodynamical scaling, one would expect a weaker zonally asymmetrical circulation as a result of global warming. Vecchi et al. (2006) found a weakening trend of the observed equatorial sea level pressure (SLP) gradient (the difference in SLP between the East Pacific cold tongue region (5°S-5°N, 160°-80°W) and the WPWP (5°S-5°N, 80°-160°E); dSLP), and attributed it to global warming-induced slowdown of the Walker circulation (the zonally asymmetrical circulation over the Pacific). In this section, we look into these aspects of the simulations examined here. The changes in dSLP in response to different perturbations are given in Table 1. Despite an overall weaker circulation as measured in the spatial variance of M_c, the change in dSLP is negligible in GAS. In contrast, dSLP decreases by 0.41 hPa in AERO, while the tropics-wide zonally asymmetrical circulation strengthens. It appears that at least for this specific set of simulations, the equatorial SLP gradient does not correlate with the strength of the Walker circulation.

The spatial patterns of δSLP are plotted in Figs. 4(a) - (c). (Note that the two rectangle boxes denote the regions used for computing the equatorial SLP gradient.) SLP responds to aerosols generally by increasing in NH, and decreasing in SH (Fig. 4(a)), a pattern that is broadly consistent with weaker large-scale ascent in NH and stronger ascent in SH (Fig. 2). The resulting pressure gradient force drives the cross-equatorial northerlies in the lower troposphere. A west-east pressure gradient exist along the equator between 5°S - 5°N presumably due to the strong local aerosol-induced cooling over WPWP and neighboring lands (see Fig. 2 of MR09), giving rise to the reduction in the equatorial SLP gradient. Similar SLP changes are also present over the convective belts at 10°N and at 10°S.

Although dSLP shows little change in GAS, SLP increases by more than 1 hPa over the South Pacific (Fig. 4(b)). This is broadly consistent with the weaker ascent over SPCZ (Fig. 5). A detailed analysis similar to the one for AERO in Section 3 yields that the warming does not change the areas of the convective regions. The weakening of the zonally asymmetrical circulation is manifested partly as weaker descent over the subsidence regions. This is in qualitative agreement with the ensemble-mean response to increased CO_2 of the Intergovernmental Panel on Climate Change (IPCC) Fourth Assessment Reports (AR4) models (Vecchi and Soden 2007). However, the spatial patterns over the convective regions differ. The weakening of ascent is rather uniform across all the major convergence zones (i.e., WPWP, ITCZ and SPCZ) for the AR4 model ensemble-mean. In contrast, this model projects little change or even slight increase in ascent over the centers of the same convergence zones, and the weaker ascent takes place most notably over the east side of SPCZ, a pattern roughly opposite to that in AERO. Note that the standard AM2.1 AGCM, when coupled to a mixed-layer ocean model, behaves in the same way as the model used in this study. The standard mixed-layer model and the fully coupled model (CM2.1) participated in AR4. It would be interesting to see whether any other AR4 models deviate substantially from the ensemble-mean response. Such an effort would shed light on the robustness of the simulated regional patterns. If, as part of the overall weakening of the Walker circulation caused by global warming, the reduction in ascent is more uniform throughout the convergence zones than projected by this model, it is fully plausible that such a change would result in a reduction in dSLP.

The simulated SLP pattern in BOTH (Fig. 4(c)) agrees well with the observed trend (see Fig. 1(a) of Vecchi et al. 2006), and the spatial structure is almost entirely due to aerosols. We acknowledge that no solid conclusion can be drawn from this comparison as the model results represent the differences between two equilibrium climate states, as opposed to transient response. Nonetheless, this leads us to believe that one needs to take into account the possible role of anthropogenic aerosols when attributing the observed equatorial SLP trend.

5. Atmospheric Moist Static Energy Transport

An energetic view of aerosol-induced circulation changes can be obtained by studying how they affect atmospheric energy transport in the greater context of re-establishing the top-of-the-atmosphere (TOA) radiative balance. Fig. 6 shows that in response to aerosols, the general circulation changes in a way such that the net flow gathers energy virtually at all the SH latitudes, and the resulting cross-equatorial energy flux (0.42 PW) tends to heat up the part of the NH tropics equatorward of 20°N. The latitudes between 20 - 45°N receive an energy influx of 0.11 PW from poleward of 45°N. The energy convergence between the equator and 45°N compensates for 53% of the TOA radiative cooling posed by aerosols in NH (0.80 PW). In comparison, the tropics exports energy towards both poles in GAS. This is at least partly due to the increase in atmospheric moisture content.

6. Hydrological Response

MR09 highlighted the nonlinearity in the hydrological response to aerosols and radiatively active gases. Here, we offer a quantitative explanation for the behavior. The runoff ($P - E$, where E is evaporation) is equal to moisture convergence. Since air flow is more variable with respect to latitude than moisture content, one can express $P - E$ approximately as

$$P - E \;=\; e_s \nabla \cdot F, \tag{2}$$

where e_s is the air mass-weighted vertical-mean moisture content, and $\nabla \cdot F$ is the divergence of the vertically integrated meridional air mass flux. If one assumes that δT is the same throughout the entire tropics, and takes into account the Clausius-Clapeyron scaling of e_s, the change in runoff ($\delta(P-E)$) can be expressed as

$$\delta(P-E) \;=\; e_s\alpha\nabla\cdot F\delta T \;+\; e_s\delta(\nabla\cdot F). \tag{3}$$

The first term on the right-hand side of Eq. 3 represents a thermodynamical effect, and is proportional to δT. Since the simulated tropical-mean δT in AERO and GAS (-1.5 and 2.2 K, respectively) can approximately add up (within 10%) to that in BOTH (0.55 K) (Table 1), the thermodynamical parts of $\delta(P-E)$ of AERO and GAS are approximately linearly additive within the tropics. This leaves the second (dynamical) term as the only possible source of nonlinearity.

HS06 argued that the thermodynamical effect dominates the hydrological response to CO_2. This is presumed to be true for GAS in this study. We can estimate from the linear dependence on δT the thermodynamical part of $\delta(P-E)$ in AERO as $\delta(P-E)$ in GAS multiplied by -0.68 (the ratio of δT in AERO to that in GAS), and treat the residual as the dynamical part. The results are plotted in Fig. 7(a). It is clear that the thermodynamical effect governs the subtropical response (approximately north of 20°N and south of 20°S). The subtropics become wetter in response to aerosols. The reason is that the local divergent flow carries less moisture out of the subtropics due to lower moisture content in a colder climate. This is qualitatively consistent with the subtropical drying due to global warming (HS06). On the other hand, the dynamical effect, with its origin in aerosol-induced circulation changes, is dominant between 20°S - 20°N. Note that these are the latitudes which exhibit the strongest nonlinearity.

One can estimate the relative difference in $\delta(\nabla\cdot F)$ between AERO and BOTH from the changes in atmospheric energy transport. A linear addition of AERO and GAS would reduce the cross-equatorial flux to 0.39 PW, as compared to 0.45 PW simulated in BOTH (Fig. 6). The difference of 0.06 PW has to be made up by altering the circulation beyond what is suggested by the linear sum. The atmospheric energy flux increases by 0.16 PW in AERO from 20°S to the equator, most of which is presumed to be due to circulation changes. By assuming that the atmospheric energy flux is proportional to air mass flux (F), one estimates that $\delta(\nabla \cdot F)$ has to increase by 38% (i.e., 0.06 divided by 0.16) to reach the simulated cross-equatorial flux in BOTH. This justifies using 38% of the estimated dynamical part of $\delta(P - E)$ in AERO as an estimate of the difference in the same quantity between AERO and BOTH. When it is added to the linear sum of AERO and GAS, the agreement with BOTH is considerably improved (Fig. 7(b)). When compared to AERO, the more vigorous circulation in BOTH results in larger increase in $P - E$ south of the equator and larger reduction north. The nonlinearity in the cross-equatorial energy flux is apparently consistent with that in $P - E$. The former can be thought of as representative of the accumulated effect of circulation changes. So, although this analysis highlights the consistent roles of nonlinear circulation changes in driving the atmospheric energy transport and hydrological cycle, it does not address their origin. Ming et al. (2011b) offered an explanation of the nonlinear dynamical response based on the baroclinic instability view of the formation of the subtropical jets.

The dynamical part of AERO (Fig. 7(a)), and the sum of AERO and GAS, with or without the dynamical correction (Fig. 7(b)) show distinct local maxima at around 4°N. Although these measures differ in value, all of them are, in nature, linear combinations of the response to aerosols and that to radiatively active gases. As discussed above, the model-simulated response to both forcings, when imposed simultaneously, exhibits strong nonlinearity, implying that a linear sum of the individual responses cannot capture important characteristics of the model-simulated climate response. In particular, no similar local maximum is present in BOTH. This leads us to believe that those present in the linear sums are merely artefacts created by arbitrarily adding up two responses, which are not entirely independent of each other.

7. Concluding Remarks

The thermodynamical scaling argument dictates that the tropical-mean circulation would normally strengthen as a response to the aerosol cooling. This is borne out in the atmosphere/mixed-layer ocean GCM simulations studied here. Anthropogenic aerosols and associated radiative cooling, which are located mostly in NH, create an interhemispheric TOA radiative imbalance. The atmosphere tries to moderate the asymmetry mainly by altering the zonal-mean circulation in the tropics. This leads to weaker (stronger) convection over the NH (SH) convective regions. The resulting cross-equatorial energy flux is able to compensate partly for the radiative deficit in NH. Unlike the zonal-mean circulation, the zonally asymmetrical circulation largely follows the thermodynamical scaling in both hemispheres. The hydrological response to aerosols is thermodynamically controlled in the subtropics, and is dynamically controlled in the deep tropics. A robust outcome is that the subtropical dry regions in both hemispheres become wetter due to the aerosol cooling. The nonlinearity in the hydrological response to aerosols and radiatively active gases appears to be rooted in the nonlinear circulation changes.

It is important to note that the above conclusions are drawn mostly from the simulations performed with one single model. Although we believe that the underlying causes and physical mechanisms of the simulated tropical circulation changes are sound, and thus their qualitative characteristics are robust, major knowledge gaps still persist. Model-simulated atmospheric concentrations and radiative effects of aerosols are poorly constrained by observations. An unrealistically strong contrast in aerosol loadings between the hemispheres implies that the adjustment in the zonal-mean circulation would be less significant than suggested by the simulations, and vice versa. Absorbing aerosols affect precipitation and general circulation in a different way from purely scattering aerosols. The increased atmospheric absorption tends to suppress global-mean precipitation, with a consequence that the resulting circulation change does not scale with that in surface temperature (Ming et al. 2010). By altering a key parameter in the convection parameterization in a model similar to the one used here, Kang et al. (2008) showed that the atmospheric adjustment to an idealized interhemispherically asymmetrical forcing varies with cloud feedback, which could be highly variable across models. Another source of uncertainty is how the oceanic circulation may be altered by aerosol forcing. An analysis of fully coupled GCM experiments indicate that although the change in the total energy transport (i.e., a net cross-equatorial flux) is similar to that in the mixed-layer ocean model, approximately half of it is realized by varying the oceanic circulation, thus considerably damping the atmospheric response.

Acknowledgments.

We thank Andrew Wittenberg and Massimo Bollasina for helpful reviews on an earlier version of the manuscript.

REFERENCES

Allen, M. R. and W. J. Ingram, 2002: Constraints on future changes in the hydrological cycle. *Nature*, **419**, 224–228.

Andreae, M. O. and P. Merlet, 2001: Emissions of trace gases and aerosols from biomass burning. *Global Biogeochem. Cycles*, **15**, 955–966.

Andrews, T., P. M. Forster, O. Boucher, N. Bellouin, and A. Jones, 2010: Precipitation, radiative forcing and global temperature change. *Geophys. Res. Lett.*, **37**, doi:10.1029/2010GL043991.

Cooke, W. F., C. Liousse, H. Cachier, and J. Feichter, 1999: Construction of a $1° \times 1°$ fossil fuel emission dataset for carbonaceous aerosol and implementation and radiative impact in the ECHAM-4 model. *J. Geophys. Res.*, **104**, 22,137–22,162.

Forster, P., et al., 2007: Changes in atmospheric constituents and in radiative forcing. *Climate Change 2007: The Physical Science Basis. Contribution of Working Group I to the Fourth Assessment Report of the Intergovernmental Panel on Climate Change*, S. Solomon, D. Qin, M. Manning, Z. Chen, M. Marquis, K. B. Averyt, M. Tignor, and H. L. Miller, Eds., Cambridge University Press, Cambridge, United Kingdom and New York, NY, USA.

Ginoux, P. A., L. W. Horowitz, V. Ramaswamy, I. V. Geogdzhayev, B. N. Holben, G. Stenchikov, and X. Tie, 2006: Evaluation of aerosol distribution and optical depth in the Geophysical Fluid Dynamics Laboratory coupled model cm2.1 for present climate. *J. Geophys. Res.*, **111**, doi:10.1029/2005JD006707.

Hansen, J., et al., 2005: Efficacy of climate forcings. *J. Geophys. Res.*, **110**, doi:10.1029/2005JD005776.

Hao, W. M. and M.-H. Liu, 1994: Spatial and temporal distribution of tropical biomass burning. *Global Biogeochem. Cycles*, **8**, 495–503.

Haywood, J. M., L. J. Donner, A. Jones, and J.-C. Golaz, 2009: Global indirect radiative forcing caused by aerosols: IPCC (2007) and beyond. *Clouds in the Perturbed Climate System*, J. Heintzenberg and R. Charlson, Eds., MIT Press, Cambridge, MA, USA.

Haywood, J. M., V. Ramaswamy, and B. J. Soden, 1999: Tropospheric aerosol climate forcing in clear-sky satellite observations over the oceans. *Science*, **283**, 1299–1303.

Hegerl, G. C., et al., 2007: Understanding and attributing climate change. *Climate Change 2007: The Physical Science Basis. Contribution of Working Group I to the Fourth Assessment Report of the Intergovernmental Panel on Climate Change*, S. Solomon, D. Qin, M. Manning, Z. Chen, M. Marquis, K. B. Averyt, M. Tignor, and H. L. Miller, Eds., Cambridge University Press, Cambridge, United Kingdom and New York, NY, USA.

Held, I. M. and B. J. Soden, 2006: Robust responses of the hydrological cycle to global warming. *J. Climate*, **19**, 5686–5699.

Horowitz, L. W., 2006: Past, present, and future concentrations of tropospheric ozone and aerosols: Methodology, ozone evaluation, and sensitivity to aerosol wet removal. *J. Geophys. Res.*, **111**, doi:10.1029/2005JD006937.

Kang, S. M., I. M. Held, D. M. W. Frierson, and M. Zhao, 2008: The response of the ITCZ to extratropical thermal forcing: Idealized slab-ocean experiments with a GCM. *J. Climate*, **21**, 3521–3532.

Liu, S. C., C. Fu, C.-J. Shiu, J.-P. Chen, and F. Wu, 2009: Temperature dependence of global precipitation extremes. *Geophys. Res. Lett.*, **36**, doi:10.1029/2009GL040218.

Ming, Y. and V. Ramaswamy, 2009: Nonlinear climate and hydrological responses to aerosol effects. *J. Climate*, **22**, 1329–1339.

Ming, Y., V. Ramaswamy, and M. A. Bollasina, 2011a: A model investigation of aerosol-induced changes in monsoon circulation. *J. Climate*, in preparation.

Ming, Y., V. Ramaswamy, and G. Chen, 2011b: A model investigation of aerosol-induced changes in boreal winter extratropical circulation. *J. Climate*, submitted.

Ming, Y., V. Ramaswamy, L. J. Donner, and V. T. J. Phillips, 2006: A new parameterization of cloud droplet activation applicable to general circulation models. *J. Atmos. Sci.*, **63**, 1348–1356.

Ming, Y., V. Ramaswamy, L. J. Donner, V. T. J. Phillips, S. A. Klein, P. A. Ginoux, , and L. W. Horowitz, 2007: Modeling the interactions between aerosols and liquid water clouds with a self-consistent cloud scheme in a general circulation model. *J. Atmos. Sci.*, **64**, 1189–1209.

Ming, Y., V. Ramaswamy, and G. Persad, 2010: Two opposing effects of absorbing aerosols on global-mean precipitation. *Geophys. Res. Lett.*, **37**, doi:10.1029/2010GL042895.

Müller, J.-F., 1992: Geographical distribution and seasonal variation of surface emissions and deposition velocities of atmospheric trace gases. *J. Geophys. Res.*, **97**, 3787–3804.

Olivier, J. G. J., et al., 1996: Description of EDGAR version 2.0: A set of global emission inventories of greenhouse gases and ozone depleting substances for all anthropogenic and most natural sources on a per country basis and on a 1 × 1 degree grid. RIVM Rep. 771060 002/TNO-MEP Rep. R96/119, Natl. Inst. for Public Health and the Environ., Bilthoven, Netherlands.

Ramaswamy, V. and C.-T. Chen, 1997: Linear additivity of climate response for combined albedo and greenhouse perturbations. *Geophys. Res. Lett.*, **24**, 567–570.

Rotstayn, L. D. and U. Lohmann, 2002: Tropical rainfall trends and the indirect aerosol effect. *J. Climate*, **15**, 2103–2116.

Sobel, A. H., J. Nilsson, and L. M. Polvani, 2001: The weak temperature gradient approximation and balanced tropical moisture waves. *J. Atmos. Sci.*, **58**, 3650–3665.

Stephens, G. L. and T. D. Ellis, 2008: Controls of global-mean precipitation increases in global warming GCM experiments. *J. Climate*, **21**, 6141–6155.

The GFDL Global Atmospheric Model Development Team, 2004: The new GFDL global atmosphere and land model AM2-LM2: Evaluation with prescribed SST simulations. *J. Climate*, **17**, 4641–4673.

Vecchi, G. A. and B. J. Soden, 2007: Global warming and the weakening of the Tropical circulation. *J. Climate*, **20**, 4316–4340.

Vecchi, G. A., B. J. Soden, A. T. Wittenberg, I. M. Held, A. Leetmaa, and M. J. Harrison, 2006: Weakening of Tropical Pacific atmospheric circulation due to anthropogenic forcing. *Nature*, **441**, 73–76.

List of Tables

TABLE 1. Absolute differences in the tropical-mean surface temperature (δT; K), and relative differences in the tropical-mean precipitation ($\delta P/P$; %), convective mass flux ($\delta M_c/M_c$; %), variances of M_c ($\delta var(M_c)/var(M_c)$; %), and absolute differences in the equatorial sea level pressure gradient ($\delta(d\mathrm{SLP})$; hPa) (perturbation cases minus CONT).

	δT	$\delta P/P$	$\delta M_c/M_c$	$\delta var(M_c)/var(M_c)$	$\delta(d\mathrm{SLP})$
AERO	-1.5	-5.7	4.5	11.7	-0.41
GAS	2.2	4.8	-10.7	-19.3	0.05
BOTH	0.55	-1.4	-5.7	-7.6	-1.02

Table 2. Relative differences in the NH and SH zonal-mean and zonally asymmetrical components of $var(M_c)$ (%) (perturbation cases minus CONT).

	NH mean	NH asym.	SH mean	SH asym.
AERO	-15.8	9.3	30.4	16.0
GAS	-5.6	-17.8	-7.2	-29.5
BOTH	-23.6	-22.3	37.6	-8.6

List of Figures

FIG. 1. Differences in meridional stream function (AERO minus CONT; colored shading) superposed on the reference (CONT; contour lines) (10^9 kg s^{-1}). Clockwise circulation is positive.

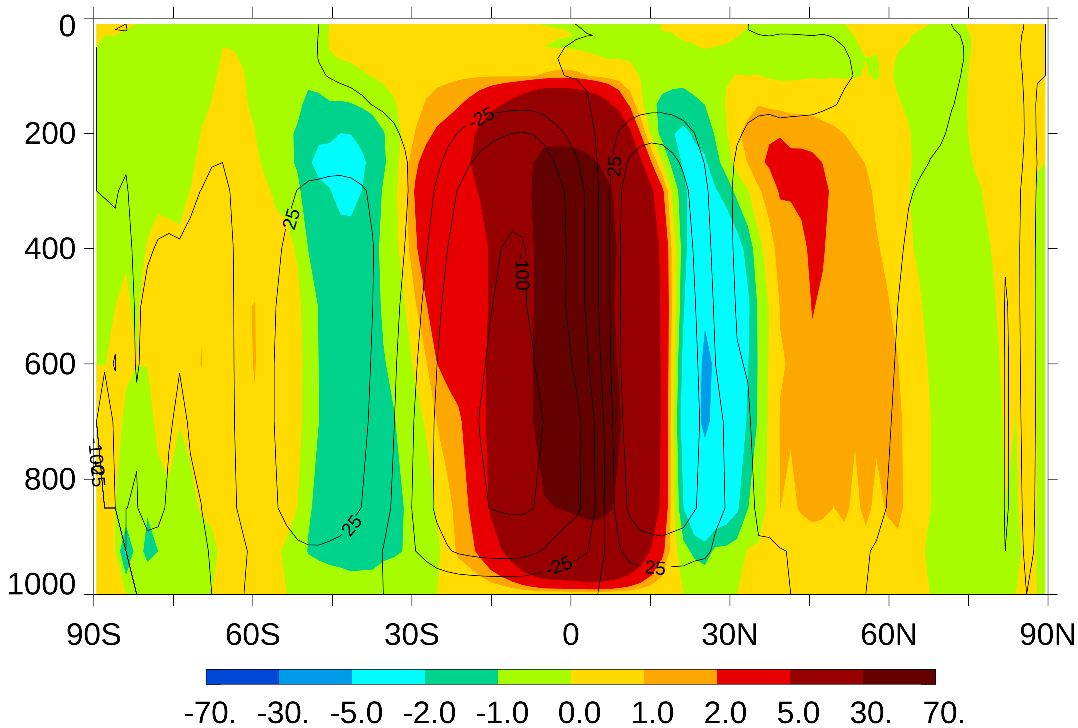

FIG. 2. Differences in grid-mean pressure velocity (ω) at 500 hPa (AERO minus CONT; colored shading with statistical significance at the 95% confidence level) superposed on the reference (CONT; contour lines) (Pa day^{-1}). Ascent is negative.

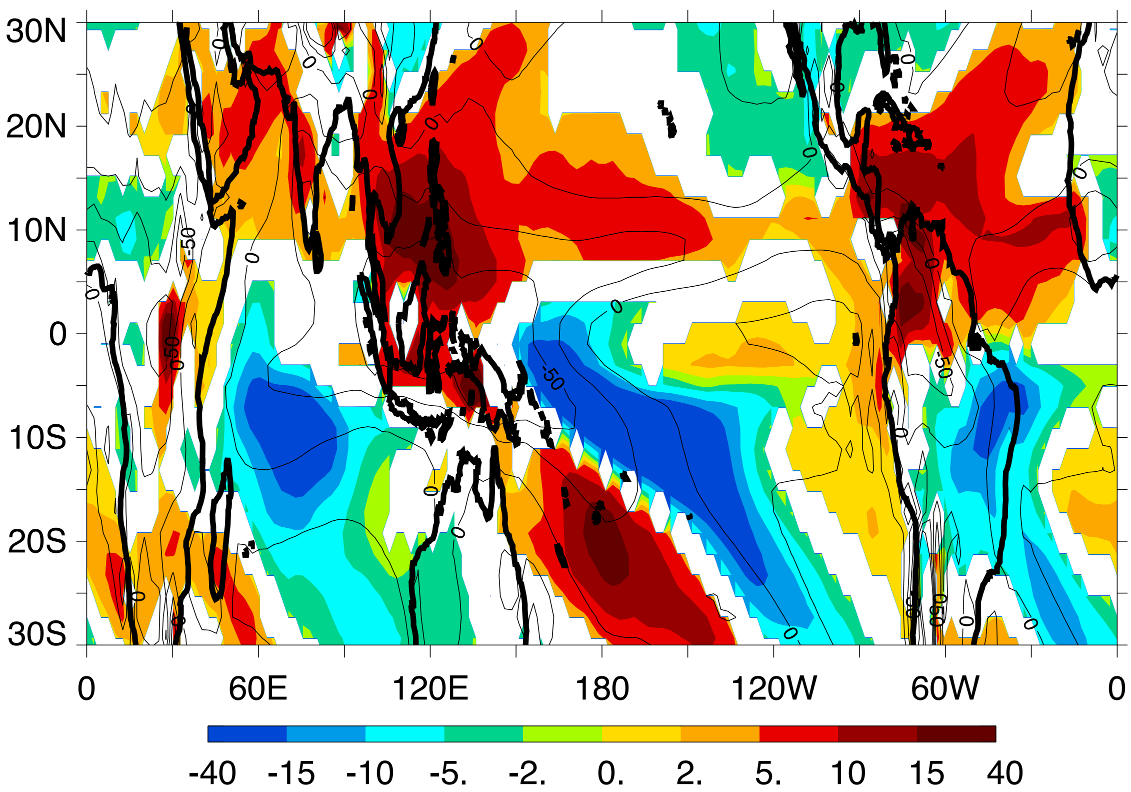

FIG. 3. Differences in the (a) total, (b) zonal-mean and (c) zonally asymmetrical convective mass fluxes at 500 hPa (M_c) (AERO minus CONT; colored shading with statistical significance at the 95% confidence level) superposed on the reference (CONT; contours) (10^{-3} kg m^{-2} s^{-1}).

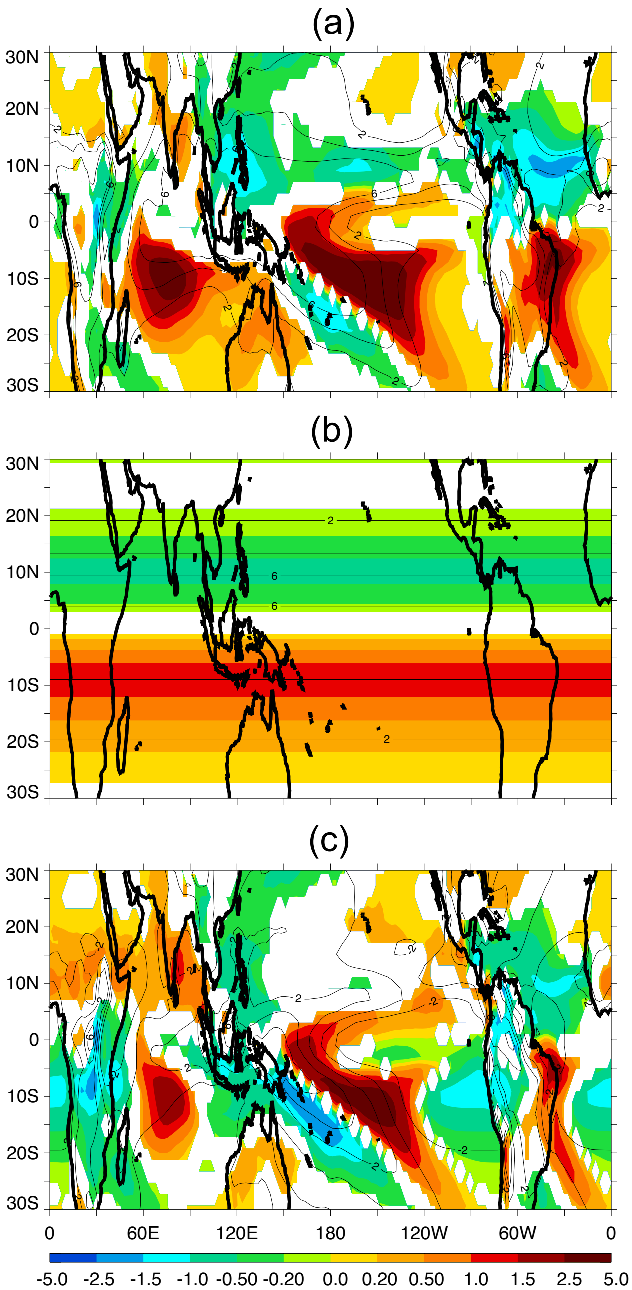

FIG. 4. Differences in sea level pressure (perturbation cases minus CONT; colored shading with statistical significance at the 95% confidence level) for (a) AERO, (b) GAS and (c) BOTH superposed on the reference (CONT; contour lines) (hPa). The rectangle boxes denote the regions used for calculating the equatorial sea level pressure gradient.

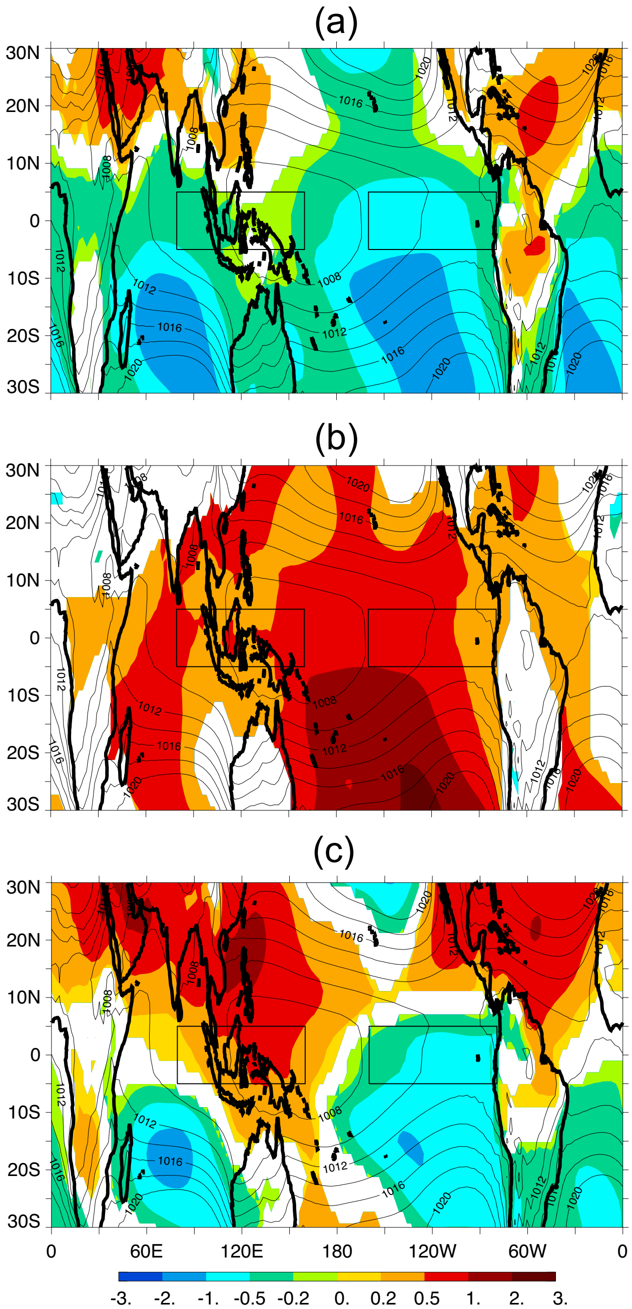

Fig. 5. Same as Fig. 2, but for GAS minus CONT.

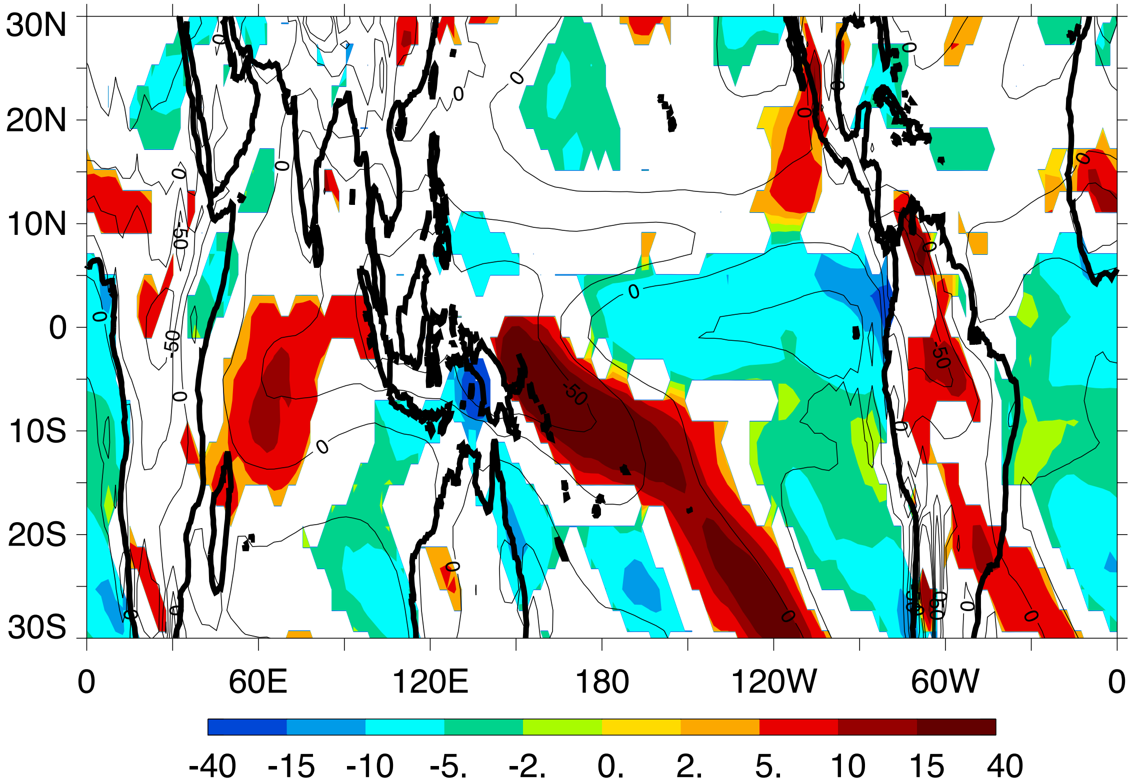

Fig. 6. Differences in zonal-mean atmospheric moist static energy transport (PW). Northward flux is positive.

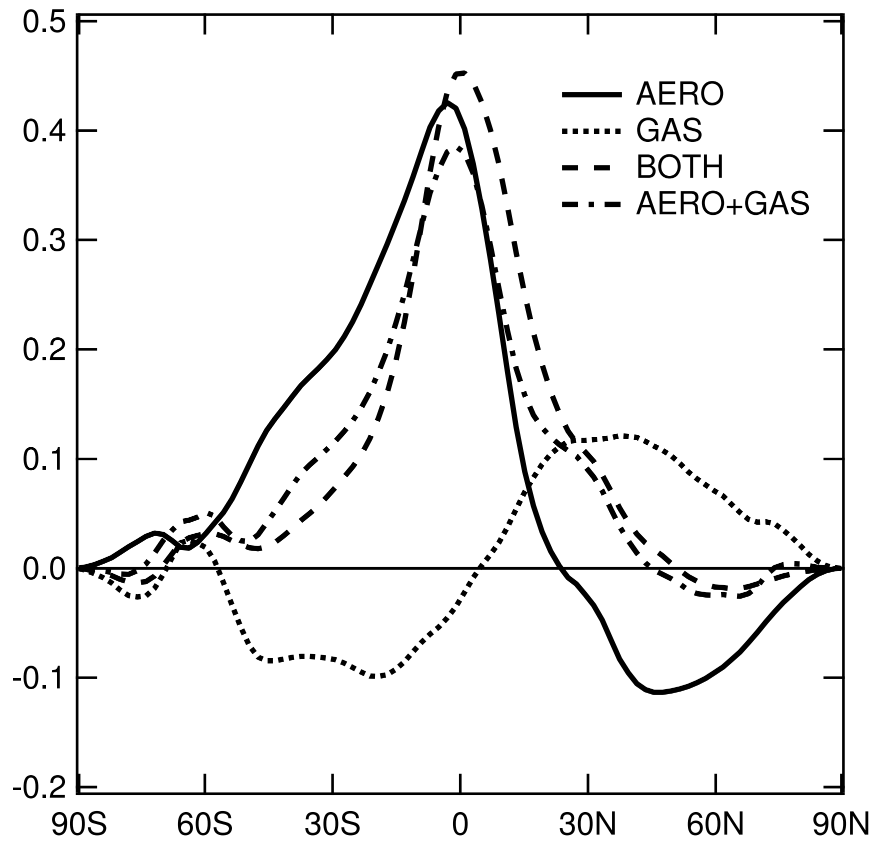

FIG. 7. Differences in zonal-mean $P - E$ (mm day^{-1}).